Journal of Zhejiang University-SCIENCE A in press
www.jzus.zju.edu.cn; www.springer.com/journal/11582
E-mail: jzus_a@zju.edu.cn

Research Article

https://doi.org/10.1631/jzus.A2500339

Effects of ultrasonic treatment on wet mineralization of cement powder

Yongsheng CHEN[1,2*], Fengping YU[3*], Yanbiao ZHU[4], Hedong LI[1,2✉], Tao WANG[5]

[1]*School of Civil Engineering and Architecture, Zhejiang Sci-Tech University, Hangzhou 310018, China*
[2]*Zhejiang Key Laboratory of Green, Digital and Intelligent (GDI) Renovation for Urban Infrastructures, China*
[3]*Zhejiang Zheneng Technology & Environment Group Co., Ltd., China*
[4]*Lanxi Tianda Environmental Protection Materials Co., Ltd., China*
[5]*State Key Laboratory of Clean Energy Utilization, Zhejiang University, Hangzhou 310012, China*

Abstract: In this study, an ultrasonic-assisted wet mineralization process was developed using ordinary Portland cement as the raw material. This approach was designed to advance the use of mineralization technologies in construction materials by simultaneously enhancing mechanical properties and mineralization efficiency. A comprehensive microstructural analysis was conducted to elucidate the underlying mineralization mechanisms facilitated by ultrasonic treatment. Furthermore, an industrial-scale implementation framework was developed to support the practical application of this technique. We found that the pH variation during the process followed three distinct stages: a rapid drop, a plateau, and a gradual decline. During the same wet mineralization period, the content of C-S-H in the ultrasonic-assisted cement suspension increased by 16%. Ultrasonic-assisted treatment improved the degree of mineralization and suppressed the growth of large crystals. Moreover, the incorporation of wet mineralization-treated suspensions into cement pastes significantly increased the compressive strength of the cementitious system. The most notable enhancement was observed when ultrasonic-assisted wet mineralization was conducted for 15 min, which resulted in a 25.78% increase in 1-day compressive strength and a 12.19% improvement in 28-day compressive strength. A 25-min ultrasonic-assisted treatment gave the greatest reduction in setting time, shortening the initial setting time by 19.46% and the final setting time by 12.98%. Based on a calculated ultrasonic mineralization energy efficiency factor, we determined that the ultrasonic-assisted wet mineralization process achieved its highest efficiency within the first 5 minutes. Prolonged mineralization resulted in a noticeable decline in mineralization efficiency.

Key words: Wet mineralization; Ultrasonic action; Cement-based material; Cement suspension

1 Introduction

Cement serves as a fundamental building material that is used extensively in modern architecture and infrastructure development. However, its manufacturing process is associated with significant emissions. Statistical data indicate that cement production contributes to about 8% of global anthropogenic CO_2 emissions, exerting a considerable influence on global warming and environmental changes (Lippiatt et al., 2020; Li and Wu, 2022). Therefore, reducing carbon emissions within the cement industry, or identifying feasible methods for capturing and storing the emitted CO_2, represents a critical strategy for addressing climate change.

Carbon capture and storage (CCS) technology, being a pivotal strategy for climate change mitigation, has attracted considerable attention and has been studied extensively across various disciplines in recent years. Cement-based materials, owing to their intrinsic alkalinity and the release of alkaline cations like Ca^{2+} during hydration, show a natural tendency toward CO_2 adsorption and mineralization (Gartner and Hirao, 2015; Ashraf, 2016; Shen et al., 2022b). Specifically, under optimal conditions of temperature, humidity, and carbon exposure, cementitious materials can undergo mineralization reactions with CO_2, forming stable compounds like calcium

✉ Hedong LI, lihedong@zstu.edu.cn
* The two authors contributed equally to this work

Received July 24, 2025; Revision accepted Dec. 23, 2025; Crosschecked

© Zhejiang University Press 2026

carbonate ($CaCO_3$), thereby achieving long-term CO_2 sequestration. Monkman et al. (2016) conducted an experiment where a controlled amount of CO_2 was introduced during the concrete mixing phase. The results showed that this method could significantly reduce both the initial and final setting times of concrete while enhancing early-age strength development. According to their findings, CO_2 reacts with the calcium components in cement particles to rapidly form micro-nano scale $CaCO_3$ particles. These particles, characterized by their high specific surface area and surface reactivity, act as nucleation centers that promote the attraction of hydration reactants, thereby accelerating the hydration process. However, the study also revealed that exceeding a certain threshold of injected CO_2 may lead to the formation of overly dense calcium carbonate coatings, which hinder further reactions and reduce overall effectiveness. In similar studies, He et al. (2017a) directly introduced CO_2 during the cement mixing phase for mineralization treatment. Although this method effectively increased CO_2 absorption in the cement system, it also led to a decline in certain mechanical properties, particularly evident in the slower development of later-stage strength. Wang et al. (2023) extended the stirring time during the carbonization process and found that the mechanical properties were improved. However, compared with cement paste that had not undergone mineralization treatment, there was still some reduction in performance.

Ultrasonic dispersion, as an external-field-assisted strengthening technology, offers a novel approach to overcome the above limitations. The ultrasonic cavitation effect has significant advantages in material synthesis and reactive mass transfer enhancement due to its unique mechano-chemical synergistic effects (Dong et al., 2016; Hamidi et al., 2017; Sulistiyono et al., 2019; Tamidi et al., 2021). Hamidi et al. (2017) confirmed through experiments on a gas-liquid system that an ultrasonic field can significantly increase the solubility of CO_2 in the liquid phase. This was attributed to the cavitation effect, which improves some properties of the liquid phase. Sulistiyono et al. (2019) introduced ultrasonic dispersion technology in the synthesis process of calcium carbonate, effectively inhibiting the phenomenon of particle agglomeration and successfully preparing nano-scale calcium carbonate with an average particle size of 64 nm. Xu et al. (2023) used an ultrasonic dispersion-assisted stirring process during the mixing of cement paste. Their results showed that the hydration rate of cement particles was significantly increased. The cavitation effect peeled off the hydration products on the surface of cement particles, and at the same time, the micro-turbulence caused by the collapse of cavitation bubbles enhanced the frequency of particle collisions. Xiong et al. (2024) confirmed that ultrasonic treatment reduced the porosity of cement paste and found that period of induction of cement hydration was shortened. Liu et al. (2021a) innovatively introduced ultrasonic dispersion during the mixing of fresh cement paste coupled with CO_2 injection. The process enhanced both the rate of uptake of CO_2 and the compressive strength of the paste, but overall mineralization efficiency remained limited due to the constraints of the mixing stage. Moreover, their study focused mainly on workability, lacking a comprehensive phase analysis of how ultrasonic treatment influences the mineralization mechanism.

Wet mineralization technology serves as an effective approach for CO_2 storage. This technology involves mainly placing solid building materials containing alkaline components in a liquid-phase environment, introducing CO_2 gas under high water-to-binder ratio conditions, and promoting reactions with alkaline cations such as Ca^{2+} and Mg^{2+} to form carbonate precipitates, thereby achieving long-term CO_2 sequestration (Lippiatt et al., 2020; Zajac et al., 2020; Shen et al., 2022a; Li et al., 2023; Mao et al., 2023; Fu et al., 2024). Under wet conditions, the solubility of CO_2 in water increases, leading to the formation of carbonic acid or bicarbonate ions. Moreover, the presence of water enhances the dispersion of solid particles and ion diffusion (Mao et al., 2023), significantly improving contact efficiency at the reaction interface and accelerating the mineralization reaction rate (Fagerlund et al., 2012; Liu et al., 2021b). However, the current mainstream wet mineralization method relies on mechanical stirring. Mechanical stirring, due to its limited dispersing ability, is unable to overcome the interfacial binding energy of the mineralized product layer (C-S-H/$CaCO_3$ complex), resulting in

continuous thickening of the product layer. This restricts the diffusion ability of Ca^{2+} and the progress of the mineralization reaction. By integrating ultrasonic dispersion technology with wet mineralization and using the energy concentration and localized strong disturbance effects of ultrasonic cavitation, we expect that the compactness of the product layer can be further reduced, the "passivation" effect of the $CaCO_3$ coating on the reaction process can be mitigated, and the conversion efficiency and uniformity of the mineralization reaction can be enhanced.

Based on established mineralization techniques, in this study we developed an ultrasonic-assisted wet mineralization process. Conventional methods relying solely on mechanical stirring generally yield limited mineralization efficiency. While previous attempts have introduced ultrasonic dispersion during the mixing of low water-to-binder ratio pastes, the high viscosity of the system and the constrained reaction time restrict the degree of mineralization, making deep treatment difficult to achieve. By integrating ultrasonic dispersion technology into a wet mineralization system, our proposed approach significantly enhances mineralization efficiency while simultaneously improving the comprehensive performance of the cement-based materials. In the experimental design, a fresh cement-water system was established, and CO_2 gas was introduced while maintaining a high water-to-binder ratio. An ultrasonic field was simultaneously applied during this process. Microstructural characterization techniques, including X-ray diffraction (XRD), Fourier transform infrared spectroscopy (FT-IR), scanning electron microscopy (SEM), and thermogravimetric analysis (TGA), were used to thoroughly examine the influence of ultrasound-assisted technology on the morphology, phase composition, and reaction pathways of the mineralized products. Furthermore, to assess its practical application potential, the cement suspension treated by ultrasound-assisted wet mineralization was incorporated into a conventional cement paste system. The early strength development, setting time and 28-day compressive strength were evaluated, and the strengthening mechanism of this technology on cement performance was analyzed. Finally, we evaluated the energy efficiency of the ultrasonic-assisted wet mineralization process and developed a scalable framework for its industrial implementation.

2 Material and experiments

The cement used in this study was ordinary Portland cement (P.O. 52.5). The oxide composition of the cement was obtained through XRF analysis (Table 1). The water used for the experiment was municipal tap water. The carbon dioxide was supplied by the Hangzhou Zhejiang Gas Co., Ltd., with a purity of 99.0%. The water-cement ratio of the cement suspension is 5:1. We elucidated the mechanism of ultrasonic-assisted wet mineralized cement suspension using pH measurement, XRD, FT-IR, TG and SEM, while assessing macroscopic performance through compressive strength and setting time. The macroscopic test specimen is cement paste. The wet mineralization of cement substitution rate is 8%, and the water-cement ratio of the cement paste specimen is 0.4. Detailed experimental specifications can be found in Section 1 of the supplementary materials.

Table 1 Composition of cement oxides

Oxide（%）	Na_2O	SO_3	MgO	K_2O	Al_2O_3	SiO_2	CaO
Cement	0.471	3.895	1.396	0.751	5.353	21.988	61.26

Table 2. Samples tested under different conditions

Sample name	Treatment	CO_2 flow rate (L/min)	Mineralized cement substitution rate (%)	Mineralization duration (min)	Total CO_2 input (L)
UC-2-5	Ultrasonic	2	8	5	10
UC-2-15	Ultrasonic	2	8	15	30
UC-2-25	Ultrasonic	2	8	25	50
MC-2-25	Non-ultrasonic	2	8	25	50

3 Results and discussion

3.1 Analysis of temperature changes

Fig. 1 illustrates the temperature evolution during the 25-min mineralization process for both the ultrasonic-assisted and the non-ultrasonic wet mineralization groups. Although both groups started at the same temperature of 20 °C, their thermal behavior exhibited significant differences.

The ultrasonic-assisted group showed substantial temperature variations, following a characteristic non-linear heating trend, with the temperature rising from an initial 20 °C to 56.8 °C. This phenomenon is attributed mainly to the thermal effects induced by ultrasonic propagation in the medium (Xiong et al., 2023): ultrasonic cavitation imparts significant kinetic energy to both fluid molecules and cement particles, converting acoustic energy into thermal energy through continuous mechanical vibration, expansion, and friction, thereby leading to a pronounced temperature increase in the system. From a kinetic perspective, the temperature change in the ultrasonic group shows distinct stages—the most notable increase occurred within the first five min, where the temperature rose rapidly from 20 °C to about 40 °C. Subsequently, the rate of heating gradually decelerated, eventually stabilizing around 56 °C.

In contrast, the non-ultrasonic group exhibited a relatively mild temperature change, remaining within a narrow range of 20–21 °C. Although both mineralization and hydration reactions of cement are exothermic in nature, the high water-to-binder ratio of the suspension effectively absorbed the reaction heat. Combined with the absence of ultrasonic energy input, this resulted in a negligible overall temperature increase in the system.

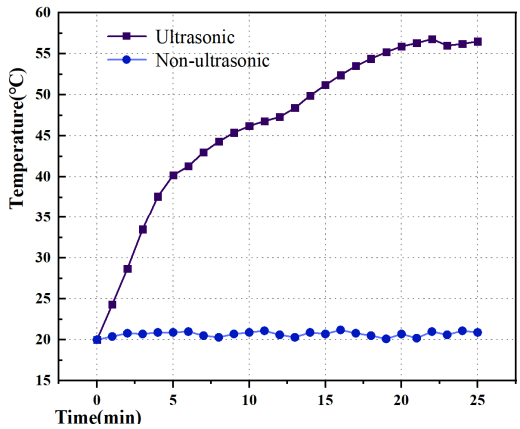

Fig. 1 Comparison of temperature changes of cement powder during ultrasonic-assisted and non-ultrasonic assisted wet mineralization

3.2 Analysis of pH changes

A comparison of pH changes between ultrasonic and non-ultrasonic wet mineralization of cement is shown in Fig. 2. The pH variation can be categorized into three distinct stages: a rapid drop, a subsequent plateau, and a final gradual decline. A detailed diagram of the mechanism of pH variation can be found in Section 2 of the supplementary material.

3.2.1 Rapid drop

Initially, the pH of the cement suspension was 11.72, which resulted from the dissolution and hydration of cement powder. Upon the onset of carbonation, the pH rapidly decreased from 11.72 to about 8, due mainly to the rapid consumption of calcium hydroxide ($Ca(OH)_2$) (Chang et al., 2018; Mehdipour et al., 2019; Wang and Chang, 2019; Goergens et al., 2020; Aghajanian et al., 2021), a product of cement hydration. During the premixing stage, cement mineral components such as tricalcium silicate (C_3S) and dicalcium silicate (C_2S) undergo hydration reactions upon contact with water, producing calcium hydroxide ($Ca(OH)_2$, referred to as (CH), and calcium silicate hydrate (C-S-H) gel, as shown in Eq. 1 and Eq. 2. CH, being the main alkaline compound, contributes to the high pH environment. When CO_2 is introduced, it dissolves in the liquid phase to form carbonic acid (H_2CO_3). Subsequently, CH reacts with H_2CO_3 to precipitate calcium carbonate ($CaCO_3$), consuming OH^- ions in the process. This reaction leads to a significant drop in the pH. The reaction rate during this stage is influenced by the mass transfer efficiency of CO_2 dissolution and the dissolution kinetics of CH.

$$3CaO \cdot SiO_2 + (n+3-x)H_2O \rightarrow xCaO \cdot SiO_2 \cdot nH_2O + (3-x)Ca(OH)_2 \quad (1)$$

$$2CaO \cdot SiO_2 + (n+2-x)H_2O \rightarrow xCaO \cdot SiO_2 \cdot nH_2O + (2-x)Ca(OH)_2 \quad (2)$$

3.2.2 Plateau

After the pH value dropped to 8–8.5, the pH plateaued, indicating that the calcium hydroxide (CH) formed during pre-mixing had been completely consumed. During this pH plateau stage, three major reaction pathways contribute to mineralization: (1) CH produced from the ongoing hydration of C_3S and C_2S continues to react with CO_2, consistent with the reactions occurring in the rapid drop; (2) C_3S directly participates in mineralization by reacting with CO_2; and (3) C_2S similarly undergoes direct mineralization with CO_2. The mineralization of CH takes precedence over that of C_3S and C_2S, meaning CH is preferentially consumed (Shen et al., 2022b). The continuous hydration of C_3S and C_2S, coupled with the concurrent mineralization of CH, C_3S, and C_2S, establishes a dynamic equilibrium. This balance continuously consumes H^+ and OH^- ions in the suspension, thereby stabilizing the pH value. From a macroscopic perspective, this corresponds to a dynamic equilibrium between the leaching rate of Ca^{2+} and the dissolution rate of CO_2. The released Ca^{2+} follows two main pathways: one portion undergoes hydration followed by mineralization, while the other participates directly in the mineralization reaction. Despite the reduction in CO_2 solubility caused by ultrasonic heating, the process simultaneously enhances the leaching kinetics of Ca^{2+}. This accelerated release of calcium ions shifts the reaction equilibrium forward, thereby increasing the CO_2 dissolution rate and overall reaction kinetics. Thus, the reaction rate was higher in the ultrasonic group than in the non-ultrasonic group at this stage. The reaction process is kinetically constrained by the dissolution rates of the mineral phases and the formation rate of the product layer (He et al., 2017b). The plateau for the ultrasonic-assisted group lasted until about 17 min, compared with only 9 min in the non-ultrasonic group (Fig. 1). Thus, ultrasonic treatment significantly extended the plateau. This phenomenon can be attributed to the surface of cement particles in the non-ultrasonic group becoming coated with a dense composite layer of C-S-H gel and $CaCO_3$ during the early plateau, forming an ion barrier that inhibits further Ca^{2+} release. In contrast, the ultrasonic-assisted wet mineralization system achieved sustained Ca^{2+} leaching rates through a dual mechanism of ultrasonic cavitation. The thermal effect enhanced ion migration and diffusion kinetics, while the mechanical stresses generated by cavitation-induced microjets and shock waves dynamically suppressed the formation of a dense product composite layer, thereby continuously exposing fresh reaction surfaces and maintaining calcium ion dissolution.

3.2.3 Gradual decline

At this stage, the surface of cement particles is coated with a significantly thicker reaction product layer, consisting of a C-S-H/$CaCO_3$ composite. The $CaCO_3$ and C-S-H gel form an intricately intertwined structure, which hinders ion diffusion and acts as an effective ion diffusion barrier. This densification of the product layer leads to a marked reduction in the leaching rate of Ca^{2+}, making its leaching efficiency lower than that of CO_2. Despite the constant rate of carbon passage, the accumulation rate of H^+ slows down during this stage. As shown in Fig. 1, the final pH values for both groups approached that of carbonic acid, indicating near saturation of CO_2 solubility in the suspension and nearing the limit of CO_2 absorption. The pH value showed a gradual downward trend. Notably, the onset of the slow descent period occurred earlier in the non-ultrasonic group than in the ultrasonic group, suggesting that regulation of the product layer structure prolongs the effective duration of the reaction.

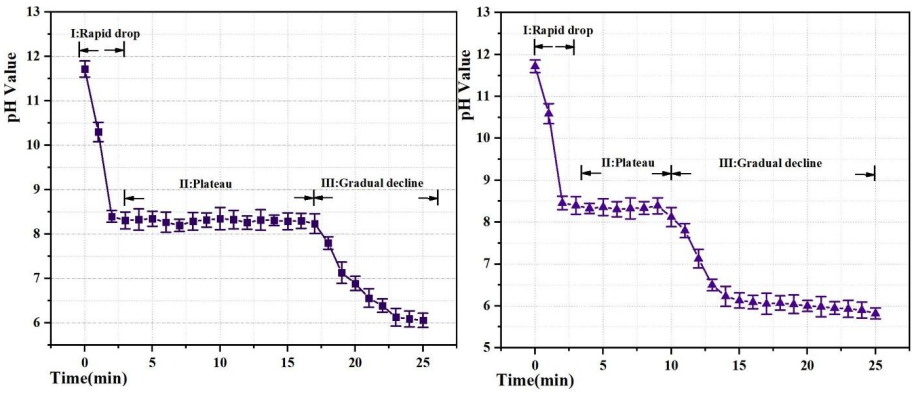

Fig 2 Comparison of pH changes of cement powder by ultrasonic-assisted and non-ultrasonic assisted wet mineralization, (A) ultrasonic-assisted, (B) non-ultrasonic assisted

3.3 XRD analysis

The results of XRD analysis of the cement powder suspensions used in wet mineralization, both with and without ultrasonic treatment, are presented in Fig. 3. The main phases identified in the cement powder during wet mineralization include calcite, C_3S, and C_2S. The data indicate that both C_3S and C_2S persisted in all samples, suggesting that the cement powder had not undergone complete mineralization. Moreover, the absence of CH in the XRD spectra confirms its full reaction, which is consistent with the results from the previous pH test. Note that calcite was the only crystalline form of calcium carbonate observed. This phenomenon can be attributed to the high water-to-binder ratio of suspension, which provides a favorable environment for sufficient contact and reaction between calcium ions and carbonate ions. As a result, the mineralization process proceeds efficiently, allowing the metastable polymorphs such as vaterite and aragonite to transform completely into the thermodynamically most stable form——calcite.

Fig. 3 shows that in the ultrasonic-assisted group (UC series), the calcite content of wet mineralization exhibited a non-linear increase trend with the extension of mineralization time. Notably, the increase of calcite during the initial 15 min of mineralization (UC-2-5 to UC-2-15) was significantly higher than the growth rate over the subsequent 10 min (UC-2-15 to UC-2-25). This attenuation in the rate of calcite formation is closely associated with the development of composite layers of reaction products: rapid consumption of CH dominates the initial mineralization phase when the cement particle surface has not yet formed a dense product layer and the Ca^{2+} leaching rate is high. As the reaction progresses, C-S-H gel deposits along with calcium carbonate form a coating that inhibits further dissolution of internal minerals, leading to a decrease in the reaction rate. The calcite peak intensity of UC-2-15 was comparable to that of UC-2-25, indicating similar extents of mineralization reaction between UC-2-15 and UC-2-25. UC-2-15 essentially represents the plateau stage depicted in Fig. 1. Effectively prolonging this homeostasis period would enhance the efficiency of wet mineralization. Both UC-2-15 and UC-2-25 exhibited significantly higher calcite content than MC-2-25. Given the established positive correlation between calcite content and mineralization duration, it can be reasonably deduced that the 15-min mechanically stirred system would produce a lower calcite content than MC-2-25. Consequently, these results confirm that under equivalent processing time (15 min), the calcite content of the 15-min ultrasonic-assisted system (UC-2-15) would exceed that of its mechanically stirred counterpart, demonstrating that ultrasonic treatment effectively enhances the overall mineralization efficiency in wet mineralization systems.

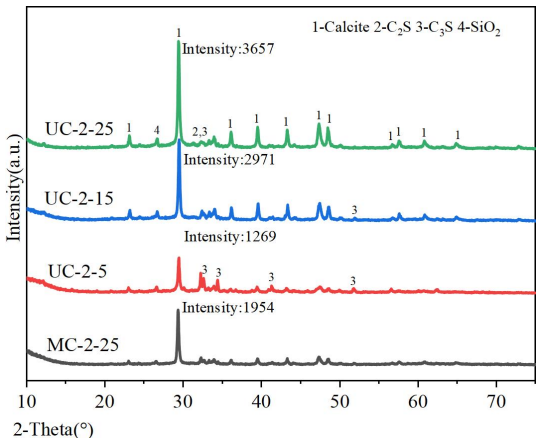

Fig. 3 XRD spectra of ultrasonic-assisted and non-ultrasonic assisted wet mineralization of cement suspensions

3.4 FT-IR analysis

The FT-IR spectra of ultrasonic-assisted and non-ultrasonic wet mineralization of cement paste suspensions are presented in Fig. 4. FT-IR spectroscopy can detect structural changes in mineralized and hydrated products, as well as other phases. According to previous studies (Shen et al., 2022b), the absorption bands around 1400, 870, and 710 cm^{-1} correspond to C-O bond vibrations, while those around 900 and 1100 cm^{-1} are associated with Si-O bond vibrations (Fernández Carrasco et al., 2012; Liu et al., 2021c). The absorption band at about 1400 cm^{-1} represents stable C-O bonds indicative of well-crystallized calcium carbonate, whereas those around 870 and 710 cm^{-1} represent less stable C-O bonds characteristic of amorphous calcium carbonate (Günther et al., 2005; Zou et al., 2015). As the ultrasonic-assisted wet mineralization time increased, the intensity of the absorption signal at 1400 cm^{-1} gradually strengthened, indicating an increase in the amount of well-crystallized calcium carbonate. Additionally, at the same carbonation time, the C-O bond absorption peak for UC-2-25 shifted to a higher wave number (1442 cm^{-1}) than that of MC-2-25 (1417cm^{-1}), suggesting a higher degree of C-O bond polymerization and a more stable crystalline structure.

FT-IR can be used for the quantitative analysis of C-S-H content and proportion during the wet mineralization process. Two overlapping absorption bands were observed within the Si-O bond region (Fig. 4). The broad band near 1000 cm^{-1} corresponds to the asymmetric tensile vibration of the Si-O bond in the initial high-calcium C-S-H. CO_2 reacts with the interlayer and defect-associated calcium in the C-S-H chain structure, forming calcium carbonate and leading to the detachment of calcium from the chains (Mao et al., 2023). The decalcified C-S-H exhibits a high degree of polymerization (Shen et al., 2022b). The wide band near 1100 cm^{-1} is attributed to the decalcification of the initial high-calcium C-S-H after mineralization, leading to low-calcium C-S-H with a higher degree of polymerization.

Previous studies have demonstrated the feasibility of decoupling FT-IR spectra for the quantitative analysis of amorphous phases such as calcium-silicate-hydrate (C-S-H) (Del Bosque et al., 2014; Mao et al., 2023). In this study, Gaussian fitting was applied to the FT-IR spectra in the 900-1200 cm^{-1} region, the range corresponding to the Si-O bond, revealing a strong correlation (Fig. 5). The deconvolution process separated the original overlapping peaks into two distinct peaks, with the peak areas representing the relative contents of high-calcium C-S-H and low-calcium C-S-H, respectively (Table 3). Additionally, the total peak area of C-S-H, which is the sum of the peak areas of high-calcium and low-calcium C-S-H, increased with prolonged ultrasonic wet mineralization time, indicating an increase in C-S-H content. Consequently, during the wet mineralization process, both mineralization and hydration reactions occur concurrently, leading to a coupled reaction between mineralization and hydration.

The total C-S-H peak areas for UC-2-5, UC-2-15, and UC-2-25 were 3656.39, 4557.21, and 4879.77, respectively, while that of MC-2-25 was 4206.14 (Table 3). The growth rate of C-S-H during the initial 5 to 15 min for ultrasonic-assisted wet mineralization was 90.08 min^{-1}, which subsequently decreased to 32.26 min^{-1} between 15 and 25 min, indicating the onset of an equilibrium stage. This suggests that the reaction rate remains highly efficient even during the plateau stage. Furthermore, under identical reaction conditions, the total peak areas of both UC-2-25 and UC-2-15 surpassed that of MC-2-25, indicating a higher C-S-H gel content in their cement suspensions. This leads to the reasonable inference that the C-S-H content of UC-2-15 would also exceed that of the mechanically stirred system with a shorter reaction

time of 15 min. This phenomenon is attributed to the ultrasonic cavitation and thermal effects, which significantly accelerates the hydration process of cement particles.

The proportion of low-calcium C-S-H in Table 3 serves as an indirect indicator of the extent of C-S-H decalcification. Sample MC-2-25 showed the highest degree of decalcification, with a low-calcium C-S-H content of 32.22%, which was slightly higher than that of UC-2-25 at 30.03%. This difference can likely be attributed to the different pH levels of the suspensions (Shen et al., 2022b). Prior research indicated that the polymerization of C-S-H gel occurs more effectively under acidic conditions. The pH of MC-2-25 was marginally lower than that of UC-2-25 (Fig. 1), thereby promoting the transformation of high-calcium C-S-H into the more polymerized low-calcium C-S-H (Shen et al., 2022b).

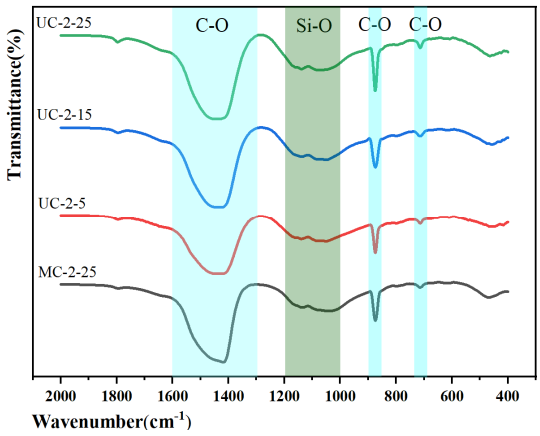

Fig. 4 FT-IR spectra of ultrasonic-assisted and non-ultrasonic assisted wet mineralization of cement suspensions

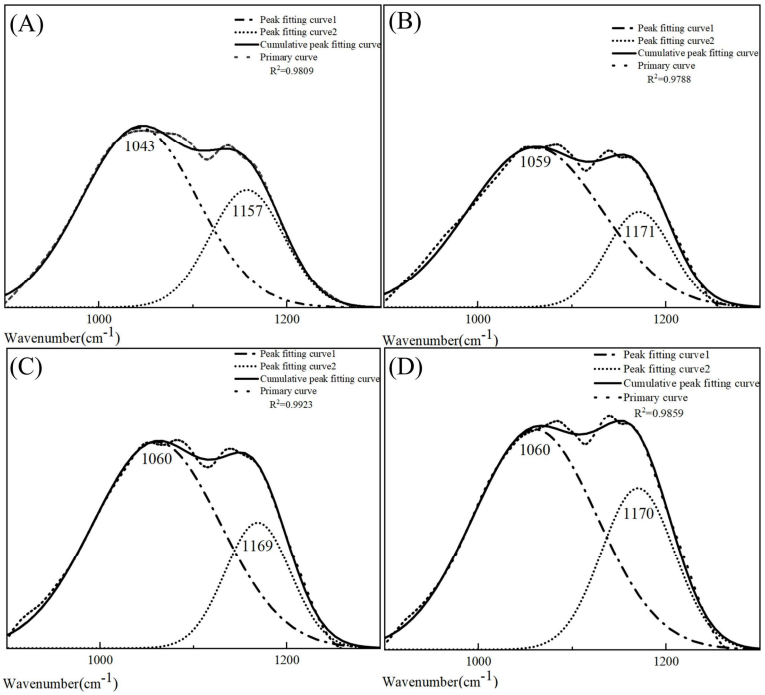

Fig. 5 FT-IR spectra split-peak fitting results in the 900 to 1200 cm^{-1} band, (A) MC-2-25, (B) UC-2-5, (C) UC-2-15, (D) UC-2-25

Table 3 Content and proportions of high-calcium C-S-H and low-calcium C-S-H in the wet mineralization process of cement powder suspensions under variable conditions

Sample name	High calcium C-S-H gel corresponds to peak area	Low calcium C-S-H gel corresponds to peak area	Total area of C-S-H peaks	High calcium C-S-H gel content percentage (%)	Low calcium C-S-H gel content percentage (%)
MC-2-25	2850.86	1355.28	4206.14	67.78	32.22
UC-2-5	2728.26	928.13	3656.39	74.62	25.38
UC-2-15	3310.65	1246.56	4557.21	72.65	27.35
UC-2-25	3414.03	1465.74	4879.77	69.97	30.03

3.5 Thermogravimetric analysis

The thermogravimetric (TG) and derivative thermogravimetric (DTG) results for the ultrasonic-assisted and non-ultrasonic wet mineralization of cement suspensions are presented in Fig. 6. The troughs in the figure are predominantly concentrated near 700 °C, corresponding to well-crystallized calcium carbonate. This indicates that the calcium carbonate formed in the cement suspension exhibits relatively high crystallinity. Additionally, the troughs in Fig. 6 progressively shift to higher temperatures, suggesting an increase in the thermal stability of the mineralized product, calcium carbonate. Notably, the stability of calcium carbonate in MC-2-25 was only marginally higher than that in UC-2-5.

By quantitatively comparing the actual CO_2 absorption of the cement suspension to its maximum potential CO_2 absorption, the degree of mineralization (α) of the cement suspension can be determined (Eq. 3). η_{expCO2} in Eq. 3 denotes the actual sequestrated CO_2 of the cement suspension and η_{theoCO2} denotes the theoretical sequestrated CO_2. The actual sequestrated CO_2 can be estimated based on the percentage of mass loss occurring near 700 °C during thermogravimetric analysis. The methodology for calculating the theoretical sequestrated CO_2 of a cement suspension is provided in Eq. 4 (Steinour, 1959; Andrade and Sanjuán, 2021).

$$\alpha = \frac{\eta_{\mathrm{exp\,CO_2}}}{\eta_{\mathrm{theo\ CO_2}}} \times 100\% \tag{3}$$

$$\eta_{\mathrm{theoCO_2}} = \frac{M_{\mathrm{CO_2}}}{M_{\mathrm{CaO}}}\left[\mu_{\mathrm{CaO}} - 0.7\mu_{\mathrm{SO_2}}\right] + 1.09\mu_{\mathrm{MgO}} + 0.71\mu_{\mathrm{Na_2O}} + 0.4675\mu_{\mathrm{K_2O}} \tag{4}$$

Here, M_{CO2} and M_{CaO} denote the molar masses of CO_2 and CaO, respectively. μ_x in Eq.4 denotes the mass percentage contents of CaO, SO_2, MgO, Na_2O and K_2O, with specific values provided in Table 1. Based on calculation, the theoretical CO_2 sequestration capacity of this cement is 48.19 g per 100 g of cement. The actual CO_2 sequestration amount for each suspension was then determined from the mass loss percentage in the TG curves (Fig. 6(A)), and the results are summarized in Table 4.

The degree of mineralization during ultrasonic wet mineralization progressively increased with the extension of carbon transfer time. Specifically, the mineralization degree for UC-2-5 was 26.56% after 5 min of ultrasonic wet mineralization and increased to 49.18% after 15 min, representing an increase of 22.62 percentage points. However, when the ultrasonic-assisted wet mineralization time was extended to 25 min, the mineralization degree reached 53.12%, which was only 3.94 percentage points higher than that observed at 15 min. These results indicate a positive correlation between the degree of mineralization and its duration. However, as mineralization proceeds, the thickening of the resulting composite product layer gradually reduces the mineralization efficiency. Under identical mineralization conditions, UC-2-15 exhibited a 9.84 percentage points higher degree of mineralization than MC-2-25. Based on the established positive correlation between the degree of mineralization and carbonation duration, it can be inferred that the 15-min mechanically stirred system would show a lower degree of mineralization than MC-2-25 and thus would be significantly lower than that of UC-2-15. Therefore, although the elevated system temperature reduces CO_2 solubility in the suspension, the cavitation-induced erosion of the product layer enhances ion diffusion efficiency, while the associated thermal effect accelerates the reaction kinetics. Collectively, these synergistic effects lead to a significant improvement in the overall degree of mineralization in the ultrasonic-assisted group.

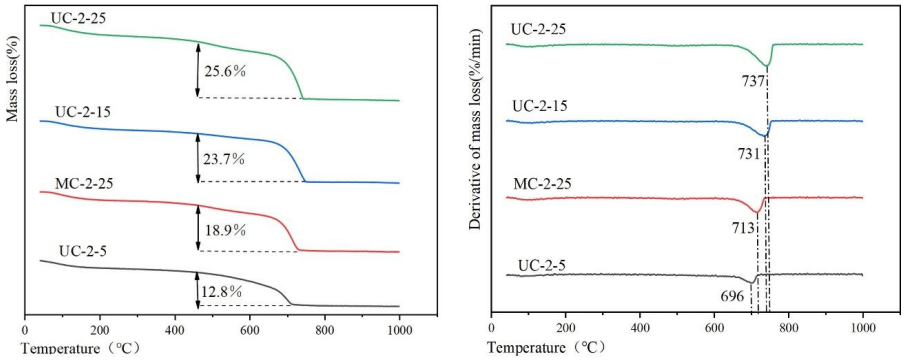

(A) TG (B) DTG

Fig. 6 TG and DTG results of ultrasonic and non-ultrasonic wet mineralization of cement suspensions

Table 4 Comparison of mass loss rate, decomposition temperature and degree of mineralization

Sample name	Mass loss rate (%)	Decomposition temperature (℃)	Degree of Mineralization (%)
MC-2-25	18.9	713	39.34
UC-2-5	12.8	696	26.56
UC-2-15	23.7	731	49.18
UC-2-25	25.6	737	53.12

3.6 SEM analysis

Scanning electron microscopy (SEM) was used to characterize the mineralized products from the ultrasonic-assisted group (UC series) and mechanical mixing group (Fig. 7). This analysis elucidated the polymorphic characteristics of calcium carbonate crystals and the evolution patterns of the product layer under different process conditions. Samples exhibited regular small cube-like calcite ($CaCO_3$) crystals with nearly 90° angles, consistent with typical calcite growth characteristics. Comparative SEM image analysis revealed that while all samples exhibited product layer agglomeration, significant differences were observed in morphology and dispersion. A continuous covering layer formed between the grains of UC-2-5 through C-S-H gel bridging (Fig. 7A), whereas continuous calcite grain accumulation was noted in UC-2-15, UC-2-25, and MC-2-25 (Fig. 7 B-D). This phenomenon can be attributed to the shorter carbonation passage time of UC-2-5, where pre-stirred C-S-H did not participate in mineralization or decalcification decomposition, resulting in reduced calcium carbonate production. Additionally, the size of calcite crystals in the ultrasonic-assisted group (UC-2-15, UC-2-25) decreased significantly, with ultrasonic treatment inhibiting the growth of larger crystals. Scale comparison based on SEM images revealed that the grain sizes in the ultrasonic-assisted wet mineralization group (Fig. 7 A-C) ranged from 100 to 200 nm, while those in the conventional wet mineralization group (without ultrasonic treatment) fell within the 300-500 nm range.

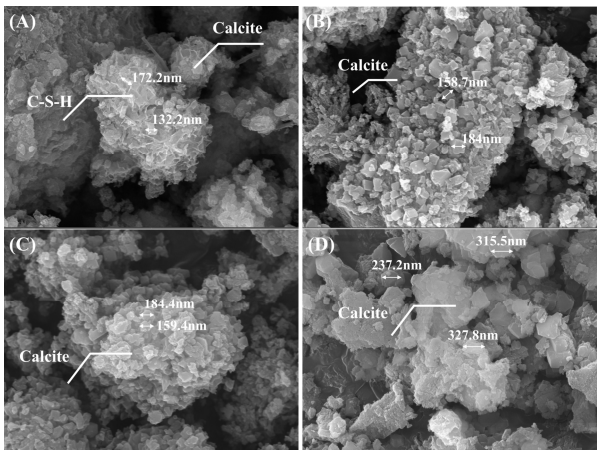

Fig. 7 SEM images of ultrasonic-assisted wet mineralization and non-ultrasonic assisted wet mineralization of cement suspensions, (A)UC-2-5, (B)UC-2-15, (C) UC-2-25, (D)MC-2-25

3.7 Setting time

The setting times for different samples are presented in Fig. 8. Comparisons of setting time, standard deviation and the rate of change relative to the control are presented in Table S7 of the supplementary material. Compared to the untreated control group, the initial setting time of all experimental groups was reduced by 6.48% to 19.46%, while the final setting time was decreased by 5.89% to 12.98%. These results indicate that wet mineralization of the cement suspension effectively

shortened the setting times of the cement paste. When comparing MC-2-25 and UC-2-25 under an identical duration of carbon transfer, UC-2-25 showed a 9.19% greater strength enhancement than MC-2-25. This improved performance can be attributed to the ultrasonic treatment generating finer crystals that provide dual benefits: a filling effect and early-stage hydration nucleation. It can be reasonably inferred that UC-2-15 would similarly exhibit higher early-age strength than its 15-min mechanically stirred counterpart. Furthermore, comparisons among the last three groups (UC-2-5, UC-2-15, UC-2-25) reveal the impact of variable ultrasonic-assisted wet mineralization times on setting time reduction. The effect of setting time reduction relative to carbon transfer time showed a nonlinear trend. Relative to UC-2-15, the initial and final setting times of UC-2-5 were further reduced by 11.01% and 5.61%, respectively. Compared with UC-2-15, the initial setting time of UC-2-25 was shortened by only 2.17%, and the final setting time by 1.48%. Evidently, when the duration of wet mineralization exceeds a certain critical threshold, the marginal benefit of reducing setting time diminishes significantly.

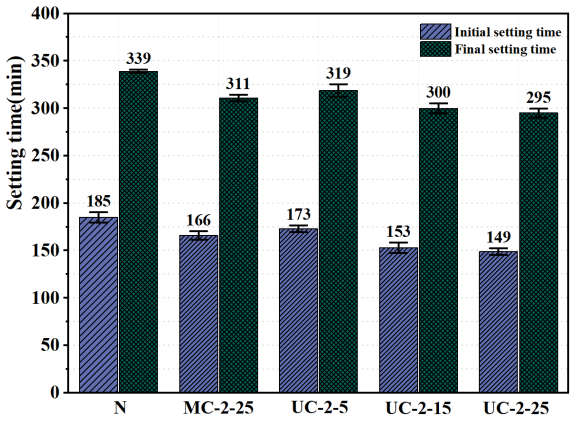

Fig. 8 Comparison of setting times

3.8 Compressive strength

The compressive strength for cement pastes partially substituted with cement suspensions at various ages are presented in Fig. 9. Comparisons of the percentage strength gain relative to the control (N) are presented in Fig. S5 of the supplementary material. The overall trend in compressive strength is clear and statistically significant. Regardless of mineralization, the compressive strength of specimens showed a non-linear increase with curing time. The strength of the experimental group after mineralization was consistently higher than that of the control group without mineralization. Across all ages, UC-2-15 demonstrated the highest compressive strength, followed by UC-2-25, while UC-2-5 exhibited the lowest strength. This may be attributed to insufficient reaction time for UC-2-5, leading to inadequate formation of $CaCO_3$ and C-S-H. Despite a longer reaction duration, group UC-2-25 exhibited the formation of a dense C–S–H/calcium carbonate composite layer on the cement particle surfaces. Although ultrasonic treatment partially disrupted this layer, its thickness and compactness continued to increase as the reaction proceeded, ultimately hindering further hydration of the unreacted inner particles. This observation aligns with the findings of Monkman et al. (2016), which indicated that an excessively thick product layer can significantly reduce ion permeability, thereby suppressing later-stage hydration and resulting in diminished gains in mechanical properties. In the present system, even with the introduction of ultrasonic agitation to delay densification, a critical threshold exists. Beyond 15 min, the continued growth of the product layer caused the reaction mechanism to shift from surface reaction control to diffusion control. Consequently, the marginal benefits in both the degree of mineralization and specimen strength development began to decline. These results confirm that the mineralization process has a well-defined optimum duration, beyond which further extension does not enhance performance.

The compressive strengths of both UC-2-15 and UC-2-25 significantly exceeded that of MC-2-25, suggesting that the inhibitory effect of the product composite layer on mechanical properties requires reaching a critical mineralization threshold. Given that the degree of mineralization of MC-2-25 remains below this critical value, it can be reasonably deduced that the 15-min mechanically stirred system with a lower degree of mineralization would not provide greater strength enhancement to the cementitious matrix than MC-2-25. Consequently, the cement paste formed by using UC-2-15 as a partial cement substitute has a higher compressive strength than the suspension liquid that was mechanically stirred for 15 min. Compared to the untreated control group (N),

the optimal performing formulation UC-2-15 showed a 25.8% increase in compressive strength at 1-day curing age, maintaining a significant 12.2% improvement after 28 days of curing. In contrast, the mechanically stirred mineralization group MC-2-25 showed corresponding gains of only 15.23% and 5.5%, respectively, with its strengthening effect merely exceeding that of UC-2-5 which underwent a shorter ultrasonic treatment among the ultrasonic-assisted groups. These results confirm that UC-2-15 provides remarkable strength enhancement to the cement paste within a relatively short mineralization period. With increasing curing age, the gain in strength of the four groups of experimental groups gradually decreased, proving that the cement suspension after wet mineralization had certain early strength characteristics. It can accelerate the hydration of cement, but the gain in strength was more limited in specimens with a 28-day curing age.

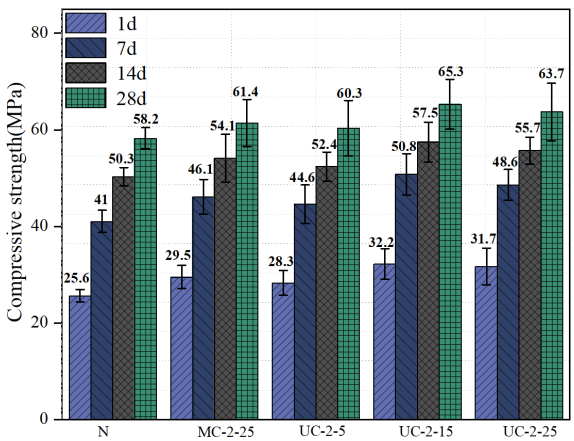

Fig 9 Compressive strength of specimens at different ages

3.9 Mechanism of ultrasonic-assisted wet mineralization

3.9.1 Mechanism of ultrasonic enhancement of mineralization efficiency

Ultrasonic waves are mechanical waves with frequencies exceeding 20 kHz, characterized by high frequency, short wavelength, and strong directivity. When ultrasonic waves propagate through a liquid medium, the periodic variation in sound pressure induces alternating compression and expansion of the medium's molecules. These cavitation nuclei undergo a three-stage dynamic evolution of expansion, contraction and collapse under the energy-driven effect of the acoustic field. During the rarefaction half-cycle, when the sound pressure falls below the tensile strength of the liquid, transient cavitation nuclei form within the liquid, leading to bubble nucleation and subsequent expansion during the same stage. In the compression half-cycle, these cavitation nuclei rapidly contract and eventually collapse (Parvizian et al., 2011; Adewuyi and Khan, 2012), generating shock jets and shock waves (Monnier et al., 1999; Abolhasani et al., 2012). This phenomenon is referred to as the cavitation effect of ultrasonic waves (Fig. S6 of supplementary material).

The ultrasonic cavitation effect plays a dual role in enhancing mineralization efficiency. The microjet causes multi-mode mechanical damage to the product composite layer (C-S-H/ $CaCO_3$) on the surface of cement particles: when the shear stress exceeds the interfacial binding energy of the composite layer, the layered structure is peeled from the matrix; the stress concentration effect induces the initiation of microcracks at the brittle calcite grain boundaries, which propagate along the crystal cleavage planes; the crack network connects to form three-dimensional permeable channels, reconstructing the pore structure and enhancing the ion diffusion efficiency, resulting in microcracks and pore channels. thereby delaying the densification process of the product composite layer. This prolongs the plateau period, maintaining a high Ca^{2+} leaching rate (Fig. 10). Previous pH measurements indicated that the onset of passivation—where mineralization efficiency begins to decline—occurs at 9 min for the non-ultrasonic group, compared to 17 min for the ultrasonic-assisted group. Furthermore, although the temperature increase induced by the ultrasonic thermal effect reduces CO_2 solubility, it significantly enhances the ion diffusion rate within the suspension. Overall, this thermal effect exerts a positive influence on mineralization efficiency. This conclusion aligns with recent research findings (Mao et al., 2023), which indicate that under consistent CO_2 flow rate conditions at temperatures below 80 °C, moderate heating promotes the degree of wet mineralization. The enhanced diffusion resulting from temperature elevation effectively compensates for the potential negative impact caused by reduced solubility, thereby improving the efficiency of the mineralization reaction.

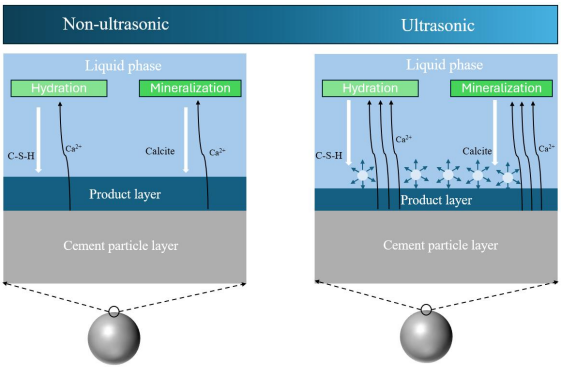

Fig 10 Stripping of the composite layer by ultrasonic action

3.9.2 Strength enhancement mechanism of ultrasonic assisted wet mineralization

The effects of ultrasonic accelerated hydration reaction and strength enhancement can be attributed to the following synergistic mechanisms. From the perspective of microscopic reaction, the shear stress induced by ultrasonic cavitation detaches some products from the product composite layer and imparts significant kinetic energy. These particles subsequently undergo intense collisions and friction, gradually reducing their size under ultrasonic refinement to reach the nanometer level (according to Fig. 10, the ultrasonic action on calcite crystals typically results in particle sizes less than 200 nm). Nanometer-sized particles exhibit higher specific surface areas and surface defect densities, which serve as active sites for the preferential adsorption of hydration reactants such as C_3S within the cement paste matrix. This reduces nucleation activation energy and accelerates the early hydration reaction process (Monkman et al., 2016). From a microscopic mechanics perspective, ultrasonic-assisted processes generate more C-S-H gels and calcite. These gels, combined with nanometer-sized calcite refined by ultrasonic treatment, exert a micro-aggregate effect, filling initial pores in the cement paste. and providing strength support, thereby enhancing both the early and later strength of the cement paste.

4 Energy Efficiency Evaluation of Ultrasonic Action

This part is presented in Section 3 of the supplementary material.

5 Industrial Application Prospects and Technical Challenges

This part is presented in Section 4 of the supplementary material.

6 Conclusions

In this study, we investigated and compared the microscopic characteristics of ultrasonic-assisted and non-ultrasonic assisted wet mineralized cement suspensions, as well as their effects on the compressive strength and setting time of cement paste after partially substituting the cement content. The following conclusions can be drawn:

(1) The change in pH of a cement suspension during wet mineralization can be systematically categorized into three distinct stages: 1) a rapid drop, where CH generated from pre-mixing hydration reacts rapidly with CO_2, causing a sharp decline in pH from 11.72 to about 8; 2) a plateau, characterized by a stable pH range of 8-8.5. Ultrasonic-assisted wet mineralization has been shown to extend this stage by 89%; 3) a gradual decline, marked by a slow decrease in pH as CO_2 approaches saturation within the suspension.

(2) Calcite was confirmed as the predominant mineral phase in the cement suspension after wet mineralization. Under identical wet mineralization durations, the calcite content was substantially increased by applying the ultrasonic-assisted method. During the process of wet mineralization, a synergistic reaction between mineralization and hydration occurs. We found that within the same mineralization time, UC-2-25 had a 16% higher C-S-H content than MC-2-25.

(3) Following substitution of a portion of the cement pastes with the wet mineralized cement suspension, the cement paste demonstrated an increase in compressive strength and exhibited enhanced early-strength properties. The maximum 1-day strength of the cement paste increased by 25.78%, the initial setting time was shortened by 19.46%, and the final setting time by 12.98%. Within the same mineralization time, the 28-day compressive strength of UC-2-25 was 3.95% higher than that of MC-2-25. UC-2-15 exhibited the maximum improvement in compressive strength. Compressive strength did not increase linearly with prolonged mineralization time, but showed a specific gain

threshold. UC-2-15 exhibited the maximum improvement in compressive strength.

(4) Ultrasonic action improved the mineralization efficiency of the suspension, and the wet mineralized suspension with ultrasonic-assisted had stronger mineralization ability. UC-2-25 exhibited the highest degree of mineralization (53.12%), surpassing MC-2-25 (non-ultrasonic wet mineralization) by 13.78% under the same mineralization time. This may be attributed to ultrasonic treatment inhibiting large crystal growth and inducing a thermal effect that accelerates the reaction rate.

Acknowledgement

The authors wish to acknowledge financial support from the Pioneer R&D Program of Zhejiang Province - China (2022C03040) and the Key Research and Development Program of Hangzhou (202204T15).

Author contributions

Yongsheng Chen: Writing-original draft, investigation, validation, formal analysis, data curation. **Fengping Yu:** Investigation, methodology, investigation, visualization. **Yanbiao Zhu**: Methodology. **Hedong Li**: Writing-review & editing, supervision, project administration, methodology, funding acquisition, conceptualization. **Tao Wang**: Conceptualization, funding acquisition.

Conflict of interest

Yongsheng CHEN, Fengping YU, Yanbiao ZHU, Hedong LI, and Tao WANG declare that they have no conflict of interest.

Reference

Adewuyi YG, Khan NE, 2012. Modeling the ultrasonic cavitation-enhanced removal of nitrogen oxide in a bubble column reactor. *AIChE Journal*, 58(8):2397-2411.

Aghajanian S, Nieminen H, Laari A, et al., 2021. Integration of a calcium carbonate crystallization process and membrane contactor–based co2 capture. *Separation and Purification Technology*, 274:119043.

Andrade C, Sanjuán MÁ, 2021. Carbon dioxide uptake by pure portland and blended cement pastes. *Developments in the Built Environment*, 8:100063.

Ashraf W, 2016. Carbonation of cement-based materials: Challenges and opportunities. *Construction and Building Materials*, 120:558-570.

Chang J, Wang D, Fang Y, 2018. Effects of mineralogical changes in bofs during carbonation on ph and ca and si leaching. *Construction and Building Materials*, 192:584-592.

Del Bosque IS, Martínez-Ramírez S, Blanco-Varela MT, 2014. Ftir study of the effect of temperature and nanosilica on the nano structure of c–s–h gel formed by hydrating tricalcium silicate. *Construction and Building Materials*, 52:314-323.

Dong Z, Yao C, Zhang Y, et al., 2016. Hydrodynamics and mass transfer of oscillating gas-liquid flow in ultrasonic microreactors. *AIChE Journal*, 62(4):1294-1307.

Fagerlund J, Highfield J, Zevenhoven R, 2012. Kinetics studies on wet and dry gas–solid carbonation of mgo and mg (oh) 2 for co 2 sequestration. *RSC advances*, 2(27):10380-10393.

Fernández Carrasco L, Torrens Martín D, Morales L, et al., 2012. Infrared spectroscopy in the analysis of building and construction materials. translators, InTech,

Fu X, Guerini A, Zampini D, et al., 2024. Storing co2 while strengthening concrete by carbonating its cement in suspension. *Communications Materials*, 5(1):109.

Gartner E, Hirao H, 2015. A review of alternative approaches to the reduction of co2 emissions associated with the manufacture of the binder phase in concrete. *Cement and Concrete Research*, 78:126-142.

Goergens J, Manninger T, Goetz-Neunhoeffer F, 2020. In-situ xrd study of the temperature-dependent early hydration of calcium aluminate cement in a mix with calcite. *Cement and Concrete Research*, 136:106160.

Günther C, Becker A, Wolf G, et al., 2005. In vitro synthesis and structural characterization of amorphous calcium carbonate. *Zeitschrift für anorganische und allgemeine Chemie*, 631(13-14):2830-2835.

Hamidi H, Mohammadian E, Haddad AS, et al., 2017. Effects of ultrasonic waves on carbon dioxide solubility in brine at different pressures and temperatures. *Petroleum Science*, 14:597-604.

He Z, Li Z, Shao Y, 2017a. Effect of carbonation mixing on co 2 uptake and strength gain in concrete. *Journal of Materials in Civil Engineering*, 29(10):04017176.

He Z, Li Z, Shao Y, 2017b. Effect of carbonation mixing on co2 uptake and strength gain in concrete. *Journal of Materials in Civil Engineering*, 29(10):04017176. https://doi.org/10.1061/(ASCE)MT.1943-5533.0002031

Li L, Wu M, 2022. An overview of utilizing co2 for accelerated carbonation treatment in the concrete industry. *Journal of CO2 Utilization*, 60:102000.

Li W, Cao M, Wang D, et al., 2023. Improving the hydration activity and volume stability of the ro phases in steel slag by combining alkali and wet carbonation treatments. *Cement and Concrete Research*, 172:107236.

Lippiatt N, Ling T-C, Pan S-Y, 2020. Towards carbon-neutral construction materials: Carbonation of cement-based materials and the future perspective. *Journal of Building Engineering*, 28:101062.

Liu L, Ji Y, Ma Z, et al., 2021a. Study on the effects of ultrasonic agitation on co2 adsorption efficiency improvement of cement paste. *Applied Sciences*, 11(15):6877.

Liu S, Shen P, Xuan D, et al., 2021b. A comparison of liquid-solid and gas-solid accelerated carbonation for

enhancement of recycled concrete aggregate. *Cement and Concrete Composites*, 118:103988.

Liu S, Zhang H, Wang Y, et al., 2021c. Carbon-dioxide-activated bonding material with low water demand. *Advances in Cement Research*, 33(5):193-196.

Mao Y, He P, Drissi S, et al., 2023. Effect of conditions on wet carbonation products of recycled cement paste powder. *Cement and Concrete Composites*, 144:105307.

Mehdipour I, Falzone G, La Plante EC, et al., 2019. How microstructure and pore moisture affect strength gain in portlandite-enriched composites that mineralize co2. *ACS Sustainable Chemistry & Engineering*, 7(15):13053-13061.

Monkman S, Macdonald M, Hooton RD, et al., 2016. Properties and durability of concrete produced using co2 as an accelerating admixture. *Cement and Concrete Composites*, 74:218-224.

Monnier H, Wilhelm A, Delmas H, 1999. The influence of ultrasound on micromixing in a semi-batch reactor. *Chemical engineering science*, 54(13-14):2953-2961.

Parvizian F, Rahimi M, Faryadi M, 2011. Macro-and micromixing in a novel sonochemical reactor using high frequency ultrasound. *Chemical Engineering and Processing: Process Intensification*, 50(8):732-740.

Saraya M, 2010. Stopping of cement hydration by various methods. *HBRC J*, 6(2):46-58.

Shen P, Lu J, Zhang Y, et al., 2022a. Preparation aragonite whisker-rich materials by wet carbonation of cement: Towards yielding micro-fiber reinforced cement and sequestrating co2. *Cement and Concrete Research*, 159:106891.

Shen P, Zhang Y, Jiang Y, et al., 2022b. Phase assemblance evolution during wet carbonation of recycled concrete fines. *Cement and Concrete Research*, 154:106733.

Steinour HH, 1959. Some effects of carbon dioxide on mortars and concrete-discussion. *J. Am. Concr. Inst*, 30(2):905-907.

Tamidi A, Lau K, Khalit S, 2021. A review of recent development in numerical simulation of ultrasonic-assisted gas-liquid mass transfer process. *Computers & Chemical Engineering*, 155:107498.

Wang D, Chang J, 2019. Comparison on accelerated carbonation of β-c2s, ca (oh) 2, and c4af: Reaction degree, multi-properties, and products. *Construction and Building Materials*, 224:336-347.

Wang M, Luo S, Pham BT, et al., 2023. Effect of co2-mixing dose and prolonged mixing time on fresh and hardened properties of cement pastes. *Journal of Zhejiang University-SCIENCE A*, 24(10):886-897.

Xiong G, Wang C, Zhou S, et al., 2023. Understanding the thermal effect of power ultrasound in cement paste. *Applied Thermal Engineering*, 232:120946.

Xiong G, Ren Y, Jia X, et al., 2024. Understanding the influence of ultrasonic power on the hydration of cement paste. *Journal of Building Engineering*, 87:108996.

Xu Z, Ji Y, Ma Z, et al., 2023. Strengthening mechanism of ultrasonic action on mechanical properties of cement-based materials. *Construction and Building Materials*, 362:129788.

Zajac M, Skibsted J, Skocek J, et al., 2020. Phase assemblage and microstructure of cement paste subjected to enforced, wet carbonation. *Cement and Concrete Research*, 130:105990.

Zou Z, Bertinetti L, Politi Y, et al., 2015. Opposite particle size effect on amorphous calcium carbonate crystallization in water and during heating in air. *Chemistry of Materials*, 27(12):4237-4246.